Available online at www.sciencedirect.com
SCIENCE DIRECT®
Lithos 75 (2004) 67–87
LITHOS
www.elsevier.com/locate/lithos

Coexisting anorogenic and subduction-related metasomatism in mantle xenoliths from the Betic Cordillera (southern Spain)

Luigi Beccaluva[a,*], Gianluca Bianchini[a,b], Costanza Bonadiman[a], Franca Siena[a], Carmela Vaccaro[a]

[a] *Dipartimento di Scienze della Terra, Università di Ferrara, Corso Ercole I D'Este 32, 44100 Ferrara, Italy*
[b] *Istituto CNR di Geoscienze e Georisorse, area della ricerca di Pisa, 56124 Pisa, Italy*

Received 10 February 2003; received in revised form 8 August 2003; accepted 18 December 2003

Available online 28 March 2004

Abstract

The mantle xenolith suite from Tallante (Betic Cordillera, southern Spain) comprises peridotites equilibrated in the spinel to plagioclase stability field, ranging in composition from fertile lherzolites to harzburgites residual after partial melting events that occurred in pre-Paleozoic times. Evidence of superimposed metasomatic effects can be attributed to at least two metasomatizing agents with distinct chemical and isotopic compositions. The first was a silica-undersaturated alkaline melt, resulting in variable Light Rare Earth Elements (LREE) and Sr–Nd isotopic enrichment ($^{87}Sr/^{86}Sr = 0.70213–0.70476$; $^{143}Nd/^{144}Nd = 0.51339–0.51250$) from Depleted Mantle (DM) to Enriched Mantle (EMI) end-members. This predominant metasomatism did not form hydrous phases, secondary textures, or significant mineralogical changes, and appears to be compositionally analogous to that recorded in xenoliths and Alpine peridotite massifs of the Southern European lithospheric mantle. The second metasomatic agent was a silica-oversaturated hydrous melt, producing local (<5–10%) mantle hybridization, with the formation of amphibole/phlogopite-bearing opx-rich harzburgites containing olivine–orthopyroxenite and gabbronorite lenses. This metasomatism is characterized by Sr–Nd isotopic values representing the most extreme enriched signature ($^{87}Sr/^{86}Sr = 0.70672–0.70856$; $^{143}Nd/^{144}Nd = 0.51213–0.51211$) found in uncontaminated anorogenic basic magmas and associated mantle xenoliths throughout Europe. These Sr–Nd isotopic data closely approach those recorded in the Miocene calc-alkaline and potassic volcanism of the Betic Cordillera, suggesting that this signature could have been inherited from subduction-derived metasomatizing melts during the Tertiary orogenic events of the Betic–Alboran region. The incompatible element distribution of these xenoliths and their constituent pyroxenes is also quite unusual, showing chondrite-normalized upward convex Middle (M)REE patterns coupled with remarkable negative Sr and Eu anomalies. Incompatible element modeling indicates that the peculiar composition of clinopyroxene, orthopyroxene and plagioclase can be accounted for by the interaction between the peridotite matrix and potassic silica-oversaturated melts, approaching lamproites found in the Betic Cordillera. A comparison with analogous worldwide occurrences indicates that some distinctive characteristics of subduction-related metasomatism in mantle materials are (1) silica-oversaturation in the form of excess orthopyroxene crystallization, in association with hydrous phases; (2) high $^{87}Sr/^{86}Sr$ ratios, departing from the anorogenic mantle array; (3) particularly high $^{87}Sr/^{86}Sr$ and low $^{143}Nd/^{144}Nd$ ratios, coupled with strong negative Sr and Eu

* Corresponding author. Tel.: +39-532-293740; fax: +39-532-210161.
E-mail address: bcc@unife.it (L. Beccaluva).

0024-4937/$ - see front matter
doi:10.1016/j.lithos.2003.12.015

anomalies, indicating a significant contribution of continental terrigenous components in the source of subduction-related metasomatizing agents.

Keywords: Mantle xenoliths; Subduction-related; Metasomatism; Betic Cordillera

1. Introduction

Mantle metasomatism is widely considered to be a first-order process responsible for governing mineralogical, chemical and isotopic heterogeneity within the lithospheric mantle. Alkali-silicate and/or carbonatite melts have been envisaged as the most effective metasomatizing agents of the lithospheric mantle in within-plate regions (Menzies et al., 1987 and references therein; O'Reilly and Griffin, 1988; O'Reilly et al., 1991; Siena et al., 1991; Coltorti et al., 2000 and references therein). More recently, research has increasingly been focused on subduction-related metasomatism in mantle xenoliths (Takahashi, 1986; Maury et al., 1992; Kepezhinskas et al., 1995; Abe et al., 1998; Ducea and Saleby, 1998; Grégoire et al., 2001; Franz et al., 2002), although several points still remain controversial with respect to the composition of metasomatic agents, the related exchange reactions with the peridotite matrix, and the mode and scale of these processes.

In this paper, new chemical and isotopic data on mantle xenoliths and constituent minerals from the Late Pliocene volcanic center of Cabezo Negro de Tallante, Betic Cordillera (Fig. 1), are discussed in

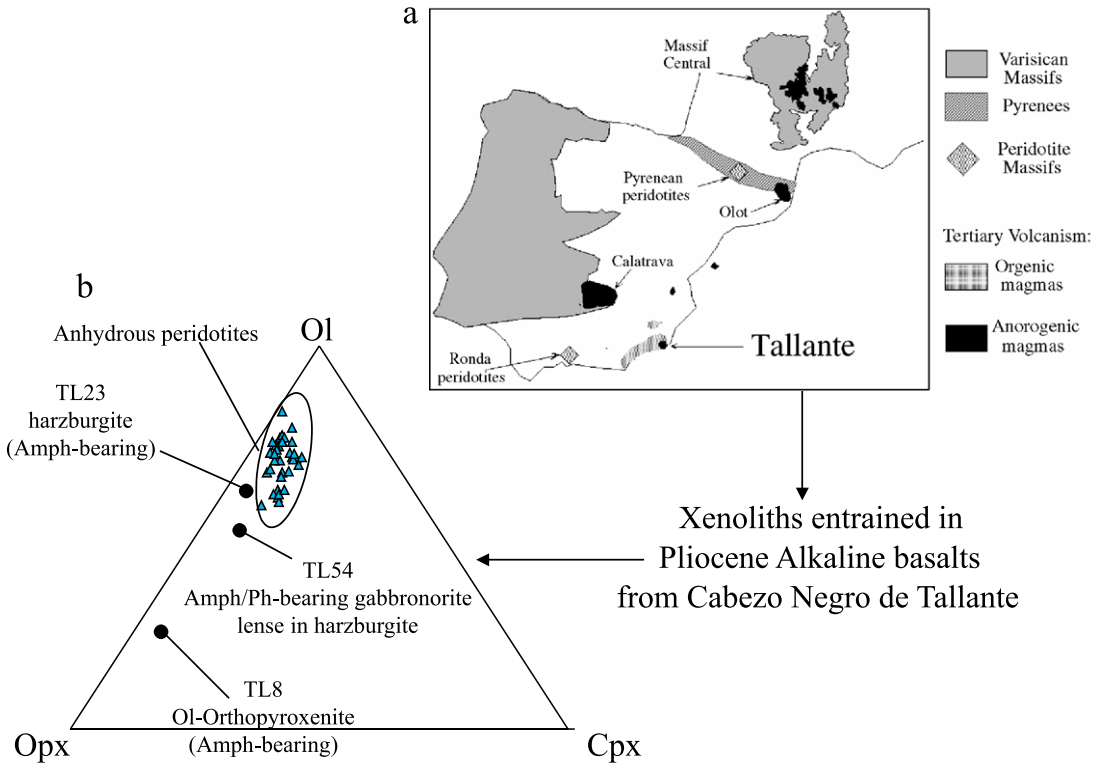

Fig. 1. (a) Sketch map of the Iberian Peninsula, reporting the location of Tertiary volcanics, Alpine-type peridotites, and Tallante. (b) Modal composition of mantle xenoliths from Tallante in terms of olivine (ol), orthopyroxene (opx) and clinopyroxene (cpx).

Table 1
Major (wt.%) and trace element (ppm) whole-rock analyses of representative mantle xenoliths from Tallante. Calculated modal compositions are also reported

	Anhydrous peridotite xenoliths													Hydrous opx-rich xenoliths		
Sample	TL 1	TL 14	TL 15	TL 16	TL 20	TL 22	TL 24	TL 26	TL 32	TL 39	TL 45	TL 52	TL 53	TL 8	TL 23	TL54
Type	Hz	Lh	Hz	Lh	Lh	Lh	Hz	Lh	Lh	Hz	Lh	Hz	Lh	Ol – Orth	Hz	Gab-Nor
SiO_2	44.15	45.55	44.34	44.51	45.16	45.02	43.82	44.42	44.82	44.48	45.66	43.66	44.58	49.15	46.42	46.51
TiO_2	0.06	0.10	0.03	0.02	0.11	0.04	0.08	0.10	0.10	0.03	0.13	0.01	0.05	0.41	0.15	1.10
Al_2O_3	1.35	2.89	0.77	1.31	3.03	1.26	1.30	2.82	2.58	0.76	3.85	0.61	1.51	6.59	2.13	8.93
FeO_{tot}	7.83	7.90	7.45	7.61	8.53	8.19	7.79	7.95	8.63	7.75	7.78	7.11	7.60	8.73	7.10	9.92
MnO	0.11	0.12	0.11	0.12	0.13	0.12	0.11	0.12	0.12	0.12	0.12	0.11	0.12	0.13	0.10	0.16
MgO	44.81	40.49	45.91	44.60	39.92	43.88	45.54	41.68	41.21	45.78	38.91	47.81	43.32	32.55	42.61	27.01
CaO	1.32	2.83	1.07	1.64	2.96	1.48	1.09	2.57	2.37	0.87	3.23	0.43	2.68	2.25	1.43	4.25
Na_2O	0.00	0.11	0.00	0.00	0.14	0.00	0.00	0.08	0.00	0.00	0.29	0.00	0.00	0.00	0.05	1.01
K_2O	0.03	0.01	0.00	0.01	0.01	0.01	0.02	0.01	0.01	0.00	0.01	0.01	0.00	0.01	0.01	0.65
P_2O_5	0.00	0.00	0.00	0.00	0.00	0.00	0.00	0.00	0.00	0.00	0.00	0.00	0.00	0.00	0.00	0.47
LOI	0.34	0.00	0.32	0.18	0.02	0.00	0.26	0.26	0.17	0.22	0.02	0.26	0.14	0.18	0.00	0.00
Ni	2314	2081	2344	2229	2223	2310	2196	2118	1688	2427	2021	2393	2281	1567	2243	1427
Co	113	110	116	113	113	106	112	116	97	113	108	114	106	89	107	85
Cr	2796	2804	2931	2827	2824	2561	2458	2990	3392	2613	2890	2509	3082	2407	1869	1848
V	46	77	40	54	74	45	45	74	68	34	73	28	67	100	46	114
Rb	4	7	2	1	1	4	1	4	1	n.d.	2	1	2	1	2	21
Ba	34	13	20	28	18	n.d.	14	16	n.d.	2	5	17	23	22	41	372
Sr	11	9	3	7	15	6	8	9	6	4	16	1	8	5	7	335
Y	1.11	2.35	0.47	0.71	2.29	0.86	0.84	2.42	2.44	0.43	3.21	0.30	1.76	9.05	2.15	11.2
Zr	10.8	5.79	2.16	2.61	4.63	3.86	7.73	5.92	5.23	1.40	11.7	1.98	2.49	43.1	18.5	95.3
Hf	0.18	0.12	0.04	0.04	0.12	0.07	0.13	0.13	0.11	0.02	0.20	0.01	0.04	0.99	0.34	2.19
Nb	0.84	0.58	0.29	0.49	0.25	0.36	0.69	0.44	0.27	0.20	0.45	0.30	0.16	0.28	0.56	25.7
Ta	0.03	0.02	0.02	0.03	0.02	0.02	0.02	0.02	0.01	0.02	0.04	0.02	0.02	0.02	0.01	1.77
La	0.88	0.27	0.10	0.36	0.34	0.15	0.63	0.30	0.37	0.09	0.41	0.10	0.14	0.78	0.43	25.5
Ce	2.20	0.60	0.25	0.64	0.50	0.34	1.32	0.82	0.85	0.16	0.96	0.31	0.57	2.61	1.66	46.3
Pr	0.24	0.11	0.03	0.07	0.11	0.04	0.17	0.11	0.14	0.02	0.18	0.03	0.09	0.59	0.35	6.18
Nd	0.88	0.52	0.15	0.25	0.51	0.19	0.65	0.53	0.63	0.10	0.88	0.11	0.42	4.23	2.52	22.5
Sm	0.20	0.19	0.04	0.05	0.18	0.06	0.19	0.19	0.19	0.03	0.33	0.03	0.15	1.87	1.12	3.87
Eu	0.05	0.08	0.02	0.02	0.07	0.03	0.05	0.09	0.07	0.01	0.13	0.01	0.05	0.24	0.12	1.02
Gd	0.24	0.29	0.06	0.07	0.26	0.09	0.19	0.27	0.26	0.04	0.47	0.05	0.21	1.93	0.73	3.61
Tb	0.04	0.06	0.01	0.01	0.05	0.02	0.03	0.06	0.05	0.01	0.09	0.01	0.04	0.33	0.10	0.47
Dy	0.23	0.35	0.07	0.09	0.33	0.11	0.18	0.33	0.32	0.06	0.57	0.06	0.30	1.67	0.42	2.34
Ho	0.05	0.09	0.02	0.02	0.08	0.03	0.04	0.08	0.08	0.02	0.13	0.01	0.07	0.34	0.07	0.41
Er	0.15	0.25	0.05	0.08	0.25	0.09	0.11	0.24	0.24	0.04	0.38	0.04	0.21	0.90	0.18	1.08
Tm	0.02	0.05	0.01	0.01	0.04	0.02	0.02	0.04	0.04	0.01	0.06	0.01	0.03	0.13	0.02	0.16
Yb	0.15	0.26	0.06	0.09	0.25	0.10	0.11	0.24	0.26	0.06	0.37	0.06	0.21	0.71	0.18	0.94
Lu	0.03	0.04	0.01	0.02	0.04	0.02	0.02	0.04	0.04	0.01	0.06	0.01	0.03	0.10	0.03	0.15
Th	0.74	0.05	0.06	0.36	0.02	0.32	0.36	0.12	0.10	0.05	0.08	0.18	0.03	0.14	0.07	7.72
U	0.13	0.03	0.02	0.11	0.01	0.09	0.09	0.04	0.05	0.02	0.03	0.05	0.02	0.04	0.03	1.64
ol	73	60	76	75	58	68	76	67	60	75	58	83	71	23	61	38
opx	21	26	20	18	27	26	19	19	28	22	24	16	18	63	33	30
cpx	5	10	4	7	11	6	4	9	10	3	11	1	11	5	4	6
sp	1	1	trace	trace	2	trace	1	2	2	trace	2	trace	trace	4	trace	2
pl	trace	3			2	trace		3			5			5	2	23
amph														<< 1	<< 1	< 1
ph																< 1

Lherzolite (Lh), harzburgite (Hz), olivine – orthopyroxenite (Ol – orth), gabbronorite (Gab-Nor). Olivine (ol), orthopyroxene (opx), clinopyroxene (cpx), spinel (sp), plagioclase (pl), amphibole (amph), phlogopite (ph).

order to distinguish the anorogenic and subduction-related metasomatic effects that appear, from preliminary investigations (Beccaluva et al., 1999, 2002), to coexist in the mantle samples of this locality. The investigated suite of xenoliths includes (1) quantitatively predominant lherzolites to harzburgites with anhydrous parageneses in the spinel (±plagioclase) peridotite facies; (2) minor xenoliths, anomalously enriched in orthopyroxene, containing amphibole and phlogopite. The first type of xenoliths displays enrichment effects related to alkaline metasomatism, which is analogous to that recorded in mantle xenoliths (Beccaluva et al., 2001a; Downes and Dupuy, 1987; Downes et al., 1992; Hartmann and Wedepohl, 1990; Zangana et al., 1997, 1998; Vaselli et al., 1995, 1996) as well as in ultramafic massifs (Reisberg et al., 1989; Bodinier et al., 1990, 1991; Downes et al., 1991; Downes, 2001 and references therein) from western and central Europe. The second type of xenoliths are silica-enriched (in the form of orthopyroxene), suggesting a possible subduction-related metasomatism.

Veined (composite) xenoliths, consisting of a peridotite matrix crosscut by kaersutite/clinopyroxene-rich veins (up to several centimeters across), are also found. These xenoliths are beyond the scope of this paper, which is focused on the distinctive features of the first two types, with the aim of better understanding the anorogenic versus subduction-related metasomatic

Table 2
Representative microprobe analyses of mineral phases from anhydrous (a) and hydrous (b) Tallante mantle xenoliths

(a)

	TL1 anhydrous harzburgite										TL16 anhydrous	
Label	12A	12E	11G	13I	11F	13G	13H	11A	13A	12B	161e	164c
Mineral	ol		opx		cpx			sp			ol	
SiO_2	40.79	40.88	55.94	55.78	52.76	51.41	50.95	–	–	–	41.19	41.24
TiO_2	–	–	0.11	0.09	0.26	0.33	0.35	0.06	0.08	0.08	–	–
Al_2O_3	–	–	3.84	3.37	3.94	4.75	4.98	49.62	47.62	49.18	–	–
FeO_{tot}	8.94	9.07	6.08	5.69	2.41	2.20	2.47	10.60	11.55	11.09	9.58	9.73
MnO	0.11	0.15	0.11	0.16	0.02	0.07	0.09	–	–	–	0.01	0.09
MgO	50.19	50.71	34.37	34.16	17.19	16.51	16.29	19.75	19.38	19.40	49.83	49.60
CaO	0.07	0.06	0.72	0.73	23.23	22.93	23.07	–	–	–	0.07	0.08
Na_2O	–	–	0.01	0.05	0.56	0.65	0.62	–	–	–	–	–
K_2O	–	–	0.00	0.00	0.00	0.00	0.00	–	–	–	–	–
Cr_2O_3	–	–	0.60	0.54	0.85	1.08	1.19	18.87	20.48	19.50	–	–
NiO	0.39	0.26	–	–	–	–	–	0.15	0.15	0.27	n.a	n.a
Total	100.49	101.12	101.79	100.58	101.23	99.92	100.01	99.06	99.26	99.52	100.68	100.74

(b)

	TL23 hydrous harzburgite											
Label	232a	231d	231c	235b	231a	231b	232c	232g	235a	232d	232e	235c
Mineral	ol		opx		cpx		sp		pl	amph		
SiO_2	41.29	41.32	55.48	55.54	51.29	52.14	–	–	54.16	43.29	43.06	43.24
TiO_2	–	–	0.31	0.30	1.09	1.01	0.13	0.14	–	2.64	2.51	1.86
Al_2O_3	–	–	3.79	3.91	6.01	5.25	48.44	48.20	29.56	14.14	13.89	14.82
FeO_{tot}	9.62	9.47	5.93	5.84	2.30	2.31	10.26	10.77	–	3.57	3.54	3.22
MnO	0.17	0.15	0.07	0.09	0.00	0.03	–	–	–	0.00	0.00	0.12
MgO	50.36	50.76	34.07	33.57	16.43	16.44	20.04	19.97	–	17.67	17.08	17.78
CaO	0.07	0.07	0.70	0.76	21.66	22.17	–	–	11.96	11.78	11.13	11.80
Na_20	–	–	0.03	0.05	0.96	0.86	–	–	4.74	3.16	3.24	2.85
K_2O	–	–	0.00	0.00	0.01	0.00	–	–	0.28	0.49	0.50	0.92
Cr_2O_3	–	–	0.42	0.68	0.86	0.86	18.97	19.90	–	1.56	1.54	1.09
NiO	0.42	0.46	–	–	–	–	0.27	0.30	–	0.14	0.14	0.16
Total	101.94	102.22	100.81	100.74	100.61	101.06	98.10	99.28	100.70	98.45	96.63	97.86

Abbreviations as in Table 1.

processes. The latter (subduction-related) process is of particular interest, also in view of the occurrence of Neogene calc-alkaline and potassic volcanism in the Betic Cordillera (Zeck et al., 1998; Benito et al., 1999; Turner et al., 1999). This study may also contribute to a better knowledge of the subcontinental mantle within the Central–Western Mediterranean area.

2. Analytical methods

Rock samples were selected to have the freshest chips and powdered in an agate mill. X-ray fluorescence (XRF) major and trace elements (Ni, Co, Cr, V, Sr, Ba and Rb) were analyzed on powder pellets, using a wavelength-dispersive automated Philips PW 1400 spectrometer at the Department of Earth Sciences (Ferrara University), according to the method by Franzini et al. (1975) and Leoni and Saitta (1976). Accuracy and precision for major elements are estimated as better than 3% for Si, Ti, Fe, Ca, and K, and 7% for Mg, Al, Mn, Na, and P; for trace elements (above 10 ppm) they are better than 7% for Rb, Sr, and V, and 15% for Ba, Ni, Co, and Cr.

Rare Earth Elements (REE), Y, Zr, Hf, Nb, Ta, Th, and U were analyzed by inductively coupled mass spectrometry (ICP-MS) at the Department of Earth Sciences (Ferrara University), using a VG Plasma

lherzolite								TL20 anhydrous lherzolite				
TL161a opx	TL163f	TL161d cpx	TL163e	TL164a	TL162a sp	TL163a	TL163c	TL20 1b ol	TL20 3e	TL20 3d opx	TL20 1a cpx	TL20 1c
55.86	56.30	52.50	53.72	52.53	–	–	–	41.24	41.16	56.03	51.38	51.01
0.03	0.03	0.09	0.13	0.18	0.03	0.03	0.05	–	–	0.13	0.78	0.81
4.19	3.79	4.14	4.51	5.57	49.96	50.73	49.83	–	–	3.06	6.24	6.37
6.12	6.33	2.27	2.26	2.14	10.88	10.58	10.24	9.83	10.18	6.18	2.17	2.36
0.12	0.06	0.11	0.04	0.08	–	–	–	0.14	0.16	0.27	0.11	0.05
33.45	34.08	16.34	16.48	15.91	19.70	19.89	19.95	48.57	48.34	33.36	15.33	15.24
0.91	0.77	22.35	22.77	22.01	–	–	–	0.06	0.05	0.64	22.85	22.46
0.03	0.04	0.77	0.86	1.03	–	–	–	–	–	0.00	0.71	0.71
0.04	0.04	0.00	0.00	0.02	–	–	–	–	–	0.00	0.00	0.01
0.53	0.49	0.97	0.99	1.18	18.38	17.68	18.63	–	–	0.21	1.23	1.07
–	–	–	–	–	–	–	–	0.34	0.30	–	–	–
101.30	101.94	99.54	101.75	100.65	98.95	98.91	98.68	100.18	100.19	99.88	100.81	100.09

TL8 hydrous olivine–orthopyroxenite									TL54 hydrous gabbronorite			
TL8 2d ol	TL8 2d opx	TL8 2f	TL8 2e sp	TL8 1a	TL8 1b pl	TL8 2a*	TL8 2c	TL8 2g	TL54 1e opx	TL54 1a amph	TL54 1b	TL54 1d
40.30	54.99	55.34	–	–	44.34	45.11	44.97	44.68	58.18	43.96	43.07	43.54
–	0.43	0.43	0.26	0.26	–	–	–	–	0.01	1.17	1.35	1.22
–	4.38	4.53	61.99	60.55	34.46	35.17	35.59	35.67	2.58	15.58	15.56	15.38
12.62	7.89	7.73	11.17	11.71	–	–	–	–	5.46	3.14	3.08	3.24
0.17	0.11	0.07	–	–	–	–	–	–	0.16	0.07	0.05	0.05
47.40	32.16	32.25	20.38	20.34	–	–	–	–	34.48	18.32	17.47	17.79
0.07	0.59	0.67	–	–	19.19	19.52	18.97	19.35	0.60	12.26	12.19	12.41
–	0.00	0.00	–	–	0.90	0.85	0.74	0.73	0.01	2.72	2.50	2.70
–	0.04	0.02	–	–	0.05	0.00	0.05	0.03	0.02	0.86	1.00	0.92
–	0.22	0.17	5.15	6.07	–	–	–	–	0.11	0.37	0.38	0.29
0.38	–	–	0.39	0.36	–	–	–	–	–	0.08	0.11	0.05
100.94	100.81	101.21	99.33	99.30	98.93	100.65	100.31	100.45	101.61	98.52	96.76	97.59

(continued on next page)

Quad2 plus. Accuracy and precision, based on the replicated analyses of samples and standards, are estimated as better than 10% for all elements well above the detection limit.

Mineral composition was obtained at the CNR-IGG Institute of Padua with a Cameca–Camebax electron microprobe (fitted with three wavelength dispersive spectrometers) at accelerating voltage of 15 kV, and specimen current of 15 nA, using natural silicates and oxides as standards. Trace element analyses on individual clinopyroxene, orthopyroxene and plagioclase grains were carried out by a Finnigan Mat single-collector double-focusing sector-field ICP-MS, coupled with laser ablation system, at the CNR-IGG Institute of Pavia. Detailed description of the technique, together with analytical protocol is given by Bottazzi et al. (1999) and Tiepolo et al. (2003). Analyses were normalized to CaO for clinopyroxene and plagioclase, and SiO_2 for orthopyroxene. NIST610 and BCR-2 glass standards were used for calibration, and the spot size was maintained at 50 μm for the entire analytical session. Accuracy has been confirmed by duplicate ICP-MS analysis of a clinopyroxene separate (0.1 g) of sample TL23, with data reproducibility generally within 10%.

Isotopic analyses on mineral separates and whole rocks were carried out at the CNR-IGG Institute of

Table 2 (*continued*)

(a)

					TL24 anhydrous harzburgite						
Label	TL20 3a	TL20 3b	TL20 3c	TL20 4a	TL243	TL242i	TL243b	TL243d	Tl243a	TL242f	TL242g
Mineral	sp	pl			ol		opx		cpx		
SiO_2	–	53.40	53.77	53.26	41.57	42.01	56.45	56.28	52.55	52.13	51.64
TiO_2	0.05	–	–	–	–	–	0.11	0.11	0.43	0.45	0.43
Al_2O_3	51.04	29.63	29.57	29.83	–	–	3.92	3.96	6.00	6.14	6.32
FeO_{tot}	10.69	–	–	–	9.68	9.15	5.93	5.99	2.15	2.49	2.09
MnO	–	–	–	–	0.01	0.11	0.20	0.24	0.03	0.04	0.17
MgO	18.84	–	–	–	49.35	49.87	33.28	33.15	15.60	15.66	15.79
CaO	–	12.74	12.44	13.04	0.06	0.05	0.74	0.74	22.76	21.95	22.39
Na_20	–	4.48	4.48	4.33	–	–	0.05	0.03	0.84	0.85	0.83
K_2O	–	0.03	0.03	0.01	–	–	0.00	0.00	0.00	0.00	0.00
Cr_2O_3	16.69	–	–	–	0.03	0.02	0.60	0.43	1.03	1.17	1.16
NiO	0.17	–	–	–	0.31	0.25	–	–	–	–	–
Total	97.49	100.29	100.29	100.48	101.02	101.46	101.27	100.95	101.39	100.87	100.81

(b)

				TL5 hydrous gabbronorite							
Label	TL54 2b	TL54 2c	TL54 2d	TL5 1e	TL5 2d	TL5 1a	TL5 1d	TL5 2c	TL5 2d	TL5 1b	TL5 1c
Mineral	ph			opx		pl				amph	
SiO_2	39.52	39.16	38.89	55.00	55.71	53.23	52.34	49.21	53.47	43.33	42.51
TiO_2	2.16	2.04	2.15	0.27	0.01	–	–	–	–	0.96	0.98
Al_2O_3	17.78	17.64	17.62	4.72	4.37	29.91	29.93	31.93	30.77	15.98	16.32
FeO_{tot}	3.03	3.02	3.06	8.66	8.67	–	–	–	–	4.91	4.97
MnO	0.07	0.00	0.04	0.20	0.22	–	–	–	–	0.08	0.17
MgO	22.99	22.77	22.61	31.78	30.61	–	–	–	–	17.02	17.55
CaO	0.06	0.08	0.01	0.42	0.63	12.75	13.06	15.86	14.53	11.56	11.24
Na_20	1.20	1.00	1.10	0.02	0.03	4.53	4.16	2.52	2.28	3.04	3.09
K_2O	8.42	8.39	8.47	0.01	0.02	0.20	0.16	0.21	0.07	0.78	0.77
Cr_2O_3	0.16	0.14	0.11	0.17	0.09	–	–	–	–	0.09	0.16
NiO	0.16	0.15	0.23	–	–	–	–	–	–	0.08	0.15
Total	95.55	94.39	94.29	101.24	100.36	100.61	99.66	99.73	101.13	97.84	97.91

Pisa; both whole-rock and mineral separates were leached with hot 6 M HCl and then digested with HF-HNO_3. Sr and Rare Earth Elements (REE) were separated by conventional techniques using cation exchange chromatographic columns, and Sr and Nd isotopic analyses were carried out on a Finnigan MAT-262 multicollector mass spectrometer. During isotopic analyses, replicate measurements ($n=23$) of the NBS987 standard gave the average value of $^{87}Sr/^{86}Sr=0.710220$ (± 5), while replicate measurements ($n=19$) of the La Jolla standard gave the average value of $^{143}Nd/^{144}Nd=0.511856$ (± 5). Raw data were adjusted to the value of $^{87}Sr/^{86}Sr=0.71025$ for NBS987 and $^{143}Nd/^{144}Nd=0.51185$ for La Jolla standard respectively. Data reproducibility, based on replicate analyses of samples, was better than 0.001%.

3. Petrography, bulk rock and mineral chemistry

A set of 39 peridotite xenoliths, lacking both alteration and host basalt infiltration, were selected for this study among a larger collection (ca. 60 samples) from the volcanic center of Cabezo Negro de Tallante. Representative major and trace element whole rock analyses are reported in Table 1. Modal compositions, calculated by mass balance based

		TL45 anhydrous lherzolite										
TL243c sp	TL242h	453F ol	453G	454A opx	451c cpx	452a	454B	453A sp	454D	453C pl	453D	453E
–	–	39.86	40.21	55.49	51.77	51.21	51.11	–	–	53.28	52.65	53.08
0.05	0.06	–	–	0.19	0.73	0.94	0.90	0.09	0.12	–	–	–
52.62	51.70	–	–	3.33	5.11	5.30	5.75	50.76	50.33	29.67	29.46	29.31
10.38	10.65	9.50	10.06	6.76	2.23	2.06	2.37	11.23	11.28	–	–	–
–	–	0.13	0.15	0.13	0.01	0.11	0.06	–	–	–	–	–
18.74	19.23	48.71	49.20	33.59	16.10	16.08	15.72	19.13	19.21	–	–	–
–	–	0.05	0.06	0.67	22.73	22.66	22.68	–	–	12.15	12.42	12.28
–	–	–	–	0.02	0.68	0.74	0.73	–	–	4.75	4.44	4.57
–	–	–	–	0.00	0.01	0.01	0.02	–	–	0.04	0.02	0.07
16.80	17.04	–	–	0.50	0.81	1.07	1.13	17.11	17.55	–	–	–
0.24	0.22	0.30	0.42	–	–	–	–	0.28	0.31	–	–	–
98.83	98.91	98.56	100.10	100.69	100.19	100.18	100.46	98.61	98.81	99.89	98.99	99.31

TL5 4b	TL5 2a ph	TL5 2b	TL5 3 a sp
43.57	37.96	38.49	0.06
1.46	1.73	1.68	0.09
15.63	18.03	18.56	63.17
5.14	5.00	4.89	12.27
0.09	0.00	0.03	–
16.98	20.86	20.58	19.64
11.67	0.04	0.02	0.01
2.94	1.03	0.93	–
0.93	8.22	8.03	–
0.10	0.40	0.34	3.17
0.07	0.07	0.11	0.28
98.57	93.35	93.65	98.69

upon the bulk rock and mineral major element analyses, are also reported. Electron microprobe and LAM ICP-MS analyses of the constituent mineral phases of representative samples are reported in Tables 2 and 3.

3.1. Anhydrous mantle xenoliths

These are quantitatively predominant, and consist of protogranular textured lherzolites (clinopyroxene up to 11%) and harzburgites (clinopyroxene down to 1%). Pyrometamorphic, glass-bearing textures (Coltorti et al., 2000) have been observed only in a few samples. The anhydrous mineral paragenesis is characterized by large (up to 1 mm) equilibrated crystals of olivine (ol), orthopyroxene (opx) and clinopyroxene (cpx). Spinel (sp), always present as lobate crystals, in several lherzolite samples shows reaction relationships with plagioclase (pl), indicating subsolidus reequilibration from spinel- to plagioclase-peridotite facies. Crystals are generally unzoned, and their major element compositional ranges are rather limited (Table 2a): Fo content between 89.4 and 90.9 for olivine; Wo 1.2–1.8, En 88.5–90.0, Fs 8.6–10.2 for orthopyroxene; Wo 47.1–49.7, En 46.5–48.8, Fs 3.7–4.5 for Cr-rich diopside clinopyroxene; Cr/(Cr+Al) between 0.17 and 0.24 for spinel; An 58.4–61.5, Ab 37.5–41.4, Or 0.1–0.4 for plagioclase.

The two-pyroxene thermometer (Brey and Koehler, 1990) gives equilibration temperatures between 830 and 970 °C. The presence of plagioclase, texturally related to spinel in several samples, suggests equilibration pressures not exceeding 8–9 kb, in accordance with the experimental boundary of Green and Hibberson (1970). This indicates that xenoliths represent the uppermost part of the lithospheric mantle just below the Moho discontinuity, which occurs at around 25 km depth under the Betic Cordillera (Banda et al., 1993).

The observed negative correlation between cpx modal abundance (and cpx/opx ratio) and olivine content from lherzolites to harzburgites conforms to that predicted by increasing degrees of partial melting of mantle materials. Coherently, whole-rock variation diagrams (Fig. 2) show that MgO (and Ni) are inversely correlated with CaO, Al_2O_3, TiO_2 and other more fusible elements which concentrate in the basaltic liquid during partial melting processes.

The depletion partial melting trend is also confirmed by the Heavy (H)REE distributions which are reliable indicators of the extent of melt extraction, being mainly hosted in clinopyroxene (Bedini and Bodinier, 1999). The least depleted lherzolites (Fig. 3a) generally display almost-flat HREE patterns (0.8–2.3 × chondrite) with variable Light (L)REE depletion ($La_N/Yb_N = 0.9–0.47$). More refractory cpx-poor lherzolites (cpx ≤ 7%) and harzburgites display comparatively lower HREE contents (0.3–0.9 × chondrite) and variable LREE enrichment (La_N/Yb_N up to 4.3; Fig. 3b) which parallel the increase of other incompatible elements, particularly Th and U (Fig. 4b). This suggests that cpx-poor mantle domains have been preferentially affected by metasomatic enrichment processes.

Trace element analyses of selected clinopyroxenes and orthopyroxenes from representative lherzolites and harzburgites are reported in Table 3. REE profiles (Fig. 5a) for clinopyroxenes of anhydrous cpx-rich lherzolites vary from moderately LREE-depleted ($La_N/Dy_N = 0.65–0.74$) or nearly flat in TL53, to decidedly more LREE-depleted in TL20 and TL45 ($La_N/Dy_N = 0.23–0.31$). In the latter samples, the appearance of a weak Eu anomaly ($Eu^* = Eu_N/[(Sm_N + Gd_N)/2] = 0.77–0.89$) is clearly related to the concomitant stability of plagioclase in their parageneses. The coexisting orthopyroxenes display a continuous depletion trend, with a steep slope from HREE to LREE. Cpx-poor lherzolites and harzburgites (Fig. 5b) show clinopyroxene REE patterns varying from comparable (TL22) to more LREE-enriched ($La_N/Sm_N = 1.1–3.3$ in samples TL1 and TL16) with respect to cpx-rich lherzolites. The orthopyroxenes of TL16 are char-

Fig. 2. Variation diagrams of SiO_2, CaO, Al_2O_3, FeO_{tot}, TiO_2, V, Ni, Sr, Zr and Y versus MgO for the studied anhydrous (grey triangles) and hydrous (●) mantle xenoliths. Compositional fields of peridotite mantle xenoliths from Central–Western Europe are reported after Downes (2001). The envelope of residual compositions after batch and fractional melting (dashed lines: at 10 and 20 kb) from a fertile lherzolite source (grey circle) is also reported for comparison after Niu (1997).

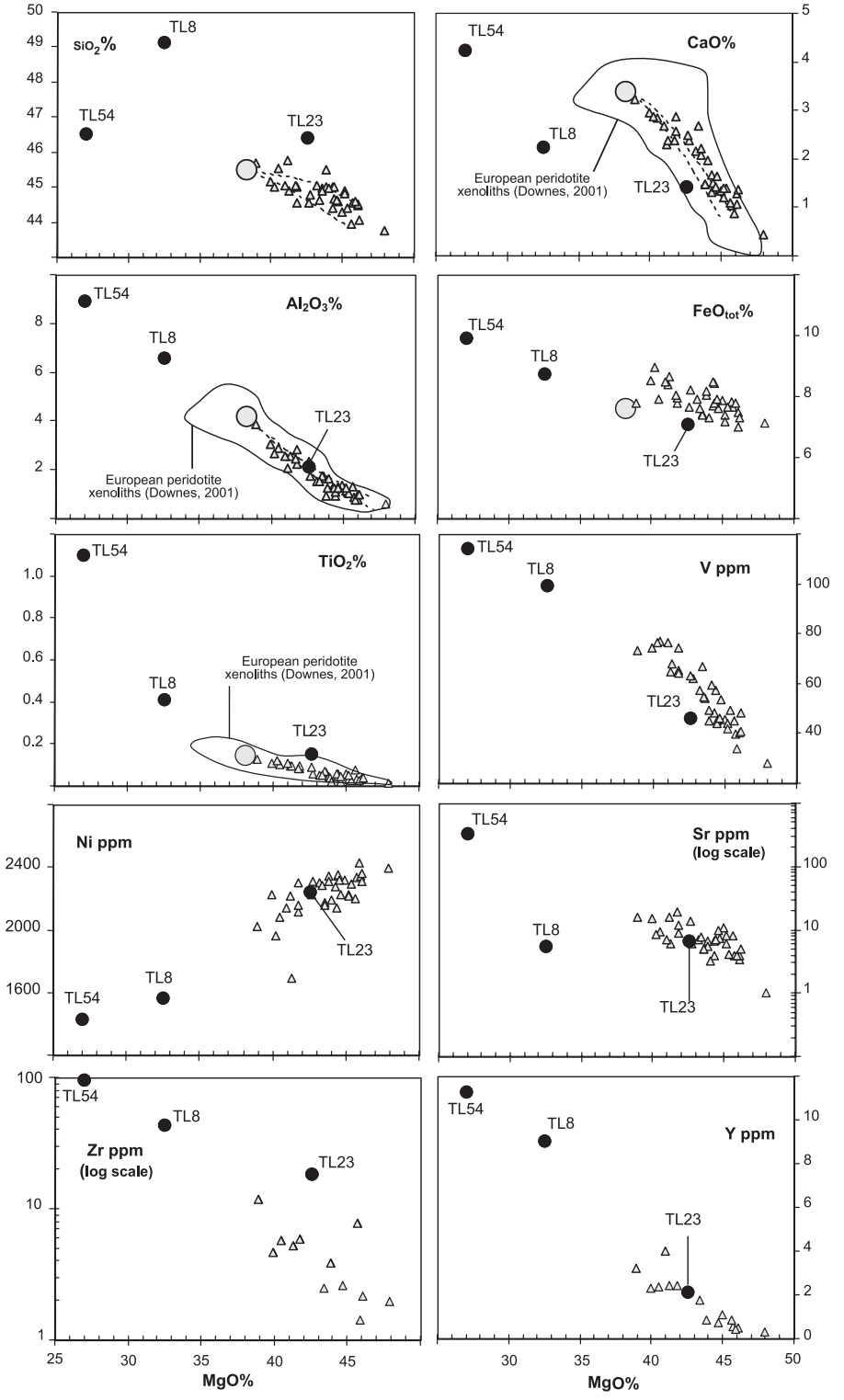
SiO2%
TL8
TL54
TL23
CaO%
European peridotite xenoliths (Downes, 2001)
Al2O3%
FeOtot%
TiO2%
V ppm
Ni ppm
Sr ppm (log scale)
Zr ppm (log scale)
Y ppm
MgO%
MgO%

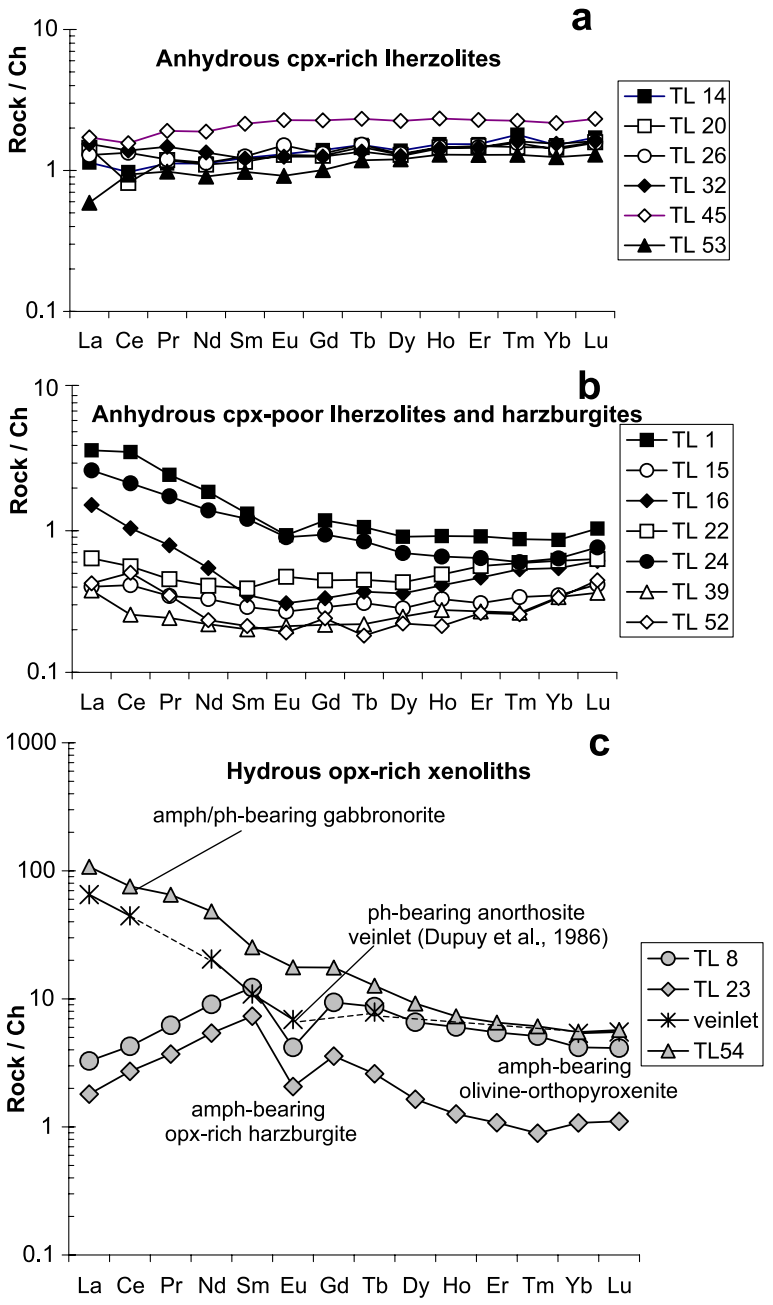

Fig. 3. Chondrite (Ch) normalized REE patterns of anhydrous (a, b) and hydrous (c) mantle xenoliths from Tallante. Normalizing factors from McDonough and Sun (1995).

acterized by V-shaped patterns with LREE enrichment, subparallel to those recorded in coexisting clinopyroxenes.

Primordial mantle-normalized incompatible element patterns of these clinopyroxenes (Fig. 6a and b) exhibit a general U and Th enrichment with distinct

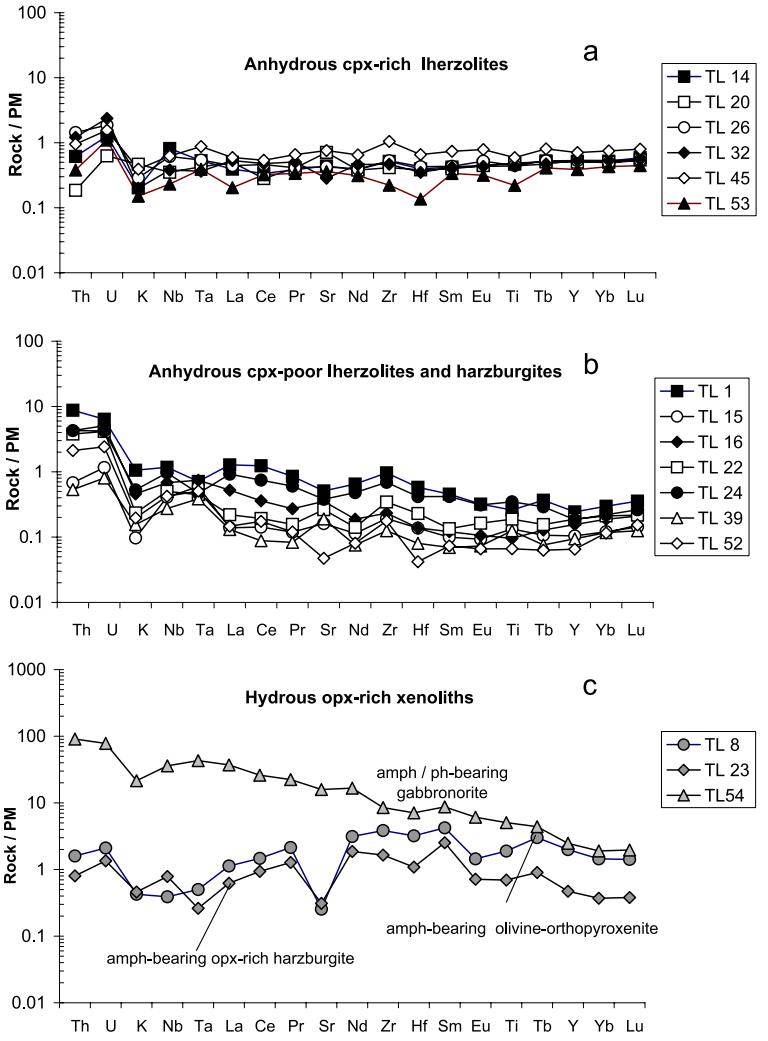

Fig. 4. Primordial mantle (PM) normalized patterns of anhydrous (a,b) and hydrous (c) mantle xenoliths from Tallante. Normalizing factors from McDonough and Sun (1995).

U positive anomaly. A significant Sr negative anomaly ($Sr^* = Sr_N/[(Ce_N + Nd_N)/2] = 0.08 - 0.20$) is recorded only in samples TL20 and TL45, which are characterized by the subsolidus appearance of plagioclase.

3.2. Hydrous mantle xenoliths

This group is characterized by the presence of hydrous phases, and varies from harzburgites to olivine–orthopyroxenite and gabbronorite lenses, all protogranular textured. Harzburgite TL23 contains microcrysts of pl and pargasitic amphibole (amph), as well as an anomalous enrichment in opx (33%). Olivine–orthopyroxenite TL8 bears minor amounts of cpx, pl, and sp, together with traces of amph, whereas thin lenses of gabbronorite in harzburgite (TL54, TL5) contain more than 20% pl, up to 30% opx and significant amounts of both amph and phlogopite (ph). The peculiar mineral parageneses, coupled with the typical protogranular texture (and lack of cumulus structure) of all these

Table 3
Representative trace element analyses (LAM ICP-MS) of clinopyroxenes, orthopyroxenes and plagioclases from Tallante peridotite xenoliths

	Anhydrous peridotite xenoliths																	
	TL1 Harzburgite			TL16 Lherzolite						TL20 Lherzolite			TL22 Lherzolite			TL45 Lherzolite		
	cpx			cpx			opx			cpx			cpx			cpx		
Rb	<0.08	0.06	0.11	<0.04	<0.05	0.14	0.16	<0.04	<0.03	<0.04	0.06	<0.03	<0.049	<0.04	<0.04	<0.03	0.06	<0.03
Ba	<0.04	0.19	0.09	<0.04	<0.05	0.09	0.14	<0.04	<0.04	0.09	<0.04	<0.03	<0.04	0.12	<0.03	<0.04	0.10	<0.03
Sr	64.4	73.2	65.2	35.2	49.8	41.3	37.6	0.27	0.05	8.89	8.71	8.71	53.3	49.6	53.5	7.46	8.60	8.53
Y	13.4	13.2	13.1	7.66	8.61	8.01	8.19	0.57	0.40	22.7	25.7	27.4	13.9	14.5	14.6	31.5	29.5	31.9
Zr	32.5	31.4	32.0	8.05	7.99	6.90	8.53	0.53	0.12	37.9	37.8	42.3	33.1	32.8	32.7	61.4	61.4	64.4
Hf	0.96	1.08	1.08	0.26	0.35	0.20	0.28	0.02	0.04	1.49	1.08	1.50	1.07	1.06	1.05	1.70	1.63	1.86
Nb	0.39	0.54	0.29	0.61	0.58	0.51	0.57	0.03	0.01	0.02	0.04	0.05	0.13	0.18	0.10	0.19	0.11	0.15
Ta	0.09	0.09	0.07	0.09	0.13	0.12	0.09	<0.002	<0.002	0.01	0.01	0.01	0.04	0.03	0.03	0.06	0.05	0.05
La	3.03	1.43	2.91	2.56	1.24	2.79	2.91	0.16	0.10	1.06	1.15	1.07	1.32	2.07	1.52	1.30	1.36	1.18
Ce	7.12	4.71	5.94	3.98	3.09	4.42	4.40	0.22	0.21	4.41	5.64	4.96	3.80	4.55	4.07	5.83	5.32	5.15
Pr	1.07	0.85	0.86	0.46	0.47	0.49	0.45	0.02	0.02	0.85	1.06	0.99	0.71	0.79	0.69	1.24	1.13	1.11
Nd	5.56	5.09	4.75	1.67	2.17	2.09	2.04	0.04	0.05	5.22	6.64	6.08	4.31	4.65	4.31	7.86	6.85	7.34
Sm	1.93	1.71	1.64	0.64	0.73	0.74	0.57	0.04	0.01	2.33	2.73	2.50	1.55	1.74	1.63	3.48	2.81	3.00
Eu	0.73	0.64	0.73	0.24	0.33	0.33	0.29	0.01	<0.005	0.73	0.87	0.86	0.74	0.68	0.70	1.07	0.85	0.97
Gd	2.26	2.23	2.06	0.93	1.21	1.01	1.02	<0.03	<0.02	3.19	3.42	3.44	2.00	2.27	2.20	4.17	3.96	4.31
Tb	0.43	0.45	0.43	0.21	0.24	0.22	0.21	0.00	0.01	0.60	0.73	0.78	0.42	0.44	0.43	0.83	0.77	0.84
Dy	2.63	2.59	2.59	1.40	1.53	1.57	1.42	0.07	0.04	3.94	4.61	4.72	2.80	2.69	2.75	5.72	4.74	5.48
Ho	0.56	0.60	0.59	0.33	0.39	0.41	0.38	0.02	0.02	0.91	1.08	1.12	0.57	0.66	0.61	1.29	1.15	1.20
Er	1.43	1.47	1.56	0.98	1.11	1.15	1.05	0.09	0.10	2.53	2.82	2.78	1.64	1.68	1.64	3.23	2.72	3.10
Tm	0.22	0.21	0.23	0.15	0.20	0.17	0.17	0.02	0.03	0.38	0.43	0.40	0.22	0.26	0.26	0.50	0.45	0.47
Yb	1.38	1.50	1.55	1.09	1.41	1.06	1.13	0.20	0.17	2.39	2.74	2.65	1.74	1.61	1.64	3.06	2.75	3.07
Lu	0.21	0.20	0.20	0.14	0.20	0.17	0.16	0.04	0.03	0.35	0.38	0.33	0.24	0.22	0.22	0.40	0.39	0.42
Pb	0.14	0.08	0.13	0.09	0.05	0.35	0.77	0.04	0.03	0.04	0.03	0.06	0.12	0.20	0.13	0.05	0.02	0.07
Th	0.52	0.13	3.58	3.28	0.40	5.62	3.47	0.47	0.36	0.13	0.10	0.08	1.10	3.21	1.78	0.06	1.16	0.05
U	0.18	0.05	1.30	1.32	0.20	2.55	1.41	0.17	0.07	0.08	0.09	0.08	0.57	1.79	0.93	0.03	0.44	0.03

Abbreviations as in Table 1.

samples, suggest that the pristine peridotite matrix was pervasively impregnated by a silica-oversaturated potassic hydrous melt, producing an excess of orthopyroxene together with plagioclase plus amphibole and phlogopite.

Microprobe analyses of harzburgite TL23 (Table 2b) show the following compositional ranges: Fo content 90.3–90.5 for olivine; Wo 1.3–1.5, En 89.6–89.8, Fs 8.8–8.9 for orthopyroxene; Wo 46.8–47.3, En 48.8–49.4, Fs 3.8–3.9 for Cr-rich diopside clinopyroxene; Cr/(Cr + Al) between 0.20 and 0.24 for spinel; An 57.0, Ab 41.4, Or 1.6 for plagioclase. Mineral compositions of olivine–orthopyroxenite TL8 are as follows: olivine, Fo 87; orthopyroxene, Wo 1.1–1.4, En 86.7–86.9, Fs 11.8–12.2; plagioclase, An 91.9–93.5, Ab 6.4–7.8, Or 0–0.3; Al-rich spinel, Cr/(Cr + Al) 0.05–0.07. Gabbronorite lenses TL5 and TL54 display comparatively wider compositional variations: plagioclase, An 60.2–78.2, Ab 21.5–38.7, Or 0.3–1.2; orthopyroxene, Wo 0.78–1.38, En 84.9–90.53, Fs 8.3–13.4; spinel, Cr/(Cr + Al) 0.03–0.23.

The mineral paragenesis of peridotite TL23 is reflected in a relatively high SiO_2 content (46.42%; Table 1), as well as CaO, FeO, TiO_2 displacement from the anhydrous xenolith group. The chemical compositions of samples TL8 and TL54, which totally differ from those of peridotites (Fig. 2), may be accounted for by a remarkable melt/peridotite interaction. The REE contents of harzburgite TL23 and olivine–orthopyroxenite TL8 are quite unusual (Fig. 3c), showing subparallel patterns characterized by upward convex Middle (M)REE with strong negative Eu anomaly and LREE depletion (La_N/Yb_N down to 0.69). Gabbronor-

						Hydrous opx-rich xenoliths									
		TL53 Lherzolite				TL23 Harzburgite									TL54 Gabbronorite
opx		cpx			opx	cpx			opx			pl			opx
<0.03	<0.03	0.05	0.03	<0.03	<0.08	0.16	0.02	0.05	<0.03	<0.03	<0.03	1.20	1.35	1.43	<0.04
<0.03	<0.04	0.28	0.04	<0.04	<0.08	0.16	0.04	0.09	<0.0	<0.04	<0.04	11.93	11.18	11.32	<0.04
<0.03	<0.03	49.9	45.7	49.3	0.12	3.94	2.59	3.04	<0.02	<0.03	0.09	175	108	122	<0.03
1.5	1.6	12.1	12.0	13.0	0.7	26.1	27.7	26.9	1.22	1.25	2.52	0.13	0.10	0.12	1.31
3.22	2.91	8.60	9.16	8.87	0.40	143	156	132	6.11	6.20	12.6	<0.07	<0.07	<0.07	5.56
0.11	0.16	0.29	0.34	0.31	0.03	5.55	4.96	5.26	0.33	0.36	0.56	0.02	<0.003	<0.006	0.24
<0.004	0.00	0.17	0.16	0.16	<0.01	0.11	0.10	0.37	<0.005	0.01	0.01	<0.006	<0.006	0.01	0.21
0.00	0.01	0.02	0.01	0.01	<0.006	0.03	0.02	0.03	<0.002	0.00	<0.002	<0.003	<0.003	<0.003	0.06
0.01	0.01	1.43	1.53	1.50	<0.005	4.28	4.00	5.23	0.01	0.01	0.08	5.44	5.02	5.05	0.06
0.02	0.03	4.02	3.98	4.07	0.02	22.77	21.24	27.59	0.03	0.03	0.38	8.25	7.32	7.91	0.18
0.01	0.01	0.60	0.66	0.69	0.01	5.73	5.68	7.15	0.01	0.01	0.11	0.92	0.66	0.80	0.03
0.03	0.02	3.38	3.48	3.87	<0.03	54.13	53.17	64.66	0.14	0.16	0.90	3.75	2.54	3.57	0.21
0.03	0.03	1.28	1.30	1.27	0.02	26.65	26.69	29.81	0.20	0.17	0.65	0.48	0.38	0.56	0.07
0.01	0.01	0.51	0.50	0.49	0.02	1.56	1.47	1.91	0.03	0.03	0.04	1.54	1.41	1.24	0.01
0.06	0.08	1.65	1.58	1.76	0.06	14.00	15.27	16.84	0.17	0.14	0.63	0.07	0.05	0.17	0.12
0.02	0.02	0.36	0.35	0.34	0.01	1.65	1.80	1.76	0.04	0.04	0.08	0.01	0.01	0.01	0.03
0.14	0.20	2.23	2.22	2.49	0.11	6.50	7.23	7.34	0.24	0.20	0.52	<0.009	<0.01	0.04	0.23
0.06	0.06	0.53	0.53	0.58	0.04	1.11	1.12	1.22	0.06	0.04	0.11	<0.002	0.01	0.00	0.06
0.19	0.26	1.49	1.45	1.62	0.11	2.36	2.40	2.38	0.17	0.19	0.26	0.01	0.03	0.01	0.19
0.04	0.05	0.22	0.23	0.23	0.02	0.30	0.29	0.28	0.03	0.03	0.06	<0.003	0.00	<0.003	0.04
0.34	0.44	1.28	1.53	1.54	0.31	1.51	1.57	1.59	0.27	0.25	0.32	0.00	<0.01	0.01	0.26
0.07	0.09	0.18	0.21	0.22	0.04	0.20	0.21	0.22	0.05	0.03	0.06	<0.002	0.01	<0.002	0.04
<0.008	0.06	0.21	0.07	0.07	<0.02	0.05	0.06	0.10	0.06	0.01	0.03	0.44	0.63	0.60	0.01
0.00	0.00	0.12	0.11	<0.02	<0.005	0.28	0.45	1.65	0.00	0.00	0.05	0.00	0.00	0.00	0.05
0.00		0.05	0.06	0.04	0.00	0.07	0.23	0.50	0.00	0.00	0.01	0.00	0.00	0.00	0.01

ite TL54 displays a remarkable LREE enrichment, closely comparable to ph-bearing anorthosite veinlets from Tallante xenoliths previously reported by Dupuy et al. (1986). Consistently, primordial mantle normalized incompatible element distributions of harzburgite TL23 and olivine orthopyroxenite TL8 (Fig. 4c) show subparallel patterns, characterized by significant Eu–Ti and Sr negative anomalies with respect to the anhydrous xenoliths.

Clinopyroxenes of harzburgite TL23 show a striking REE pattern (Fig. 5c), with highly enriched upward convex MREE and a remarkable Eu anomaly (Eu* = 0.20–0.22). Orthopyroxenes mimic the REE patterns of coexisting clinopyroxenes, displaying comparable LREE depletion and Eu negative anomalies. Incompatible element patterns of TL23 clinopyroxenes (Fig. 6c) coherently show Eu–Ti and outstanding Sr negative anomaly (Sr_N/Nd_N = 0.003–0.005).

4. Sr–Nd isotopes

Sr and Nd isotopic compositions on whole-rock and mineral separates are reported in Table 4. Data show a wide compositional range (Fig. 7) from the Depleted Mantle (DM) to the Enriched Mantle (EMI and EMII) end-members (Zindler and Hart, 1986), with $^{87}Sr/^{86}Sr$ between 0.70213 and 0.70856, and $^{143}Nd/^{144}Nd$ between 0.51339 and 0.51211. In particular, the anhydrous mantle xenoliths are in the range $^{87}Sr/^{86}Sr$ 0.70213–0.70476 and $^{143}Nd/^{144}Nd$ 0.51339–0.51250, whereas completely different isotopic compositions are shown

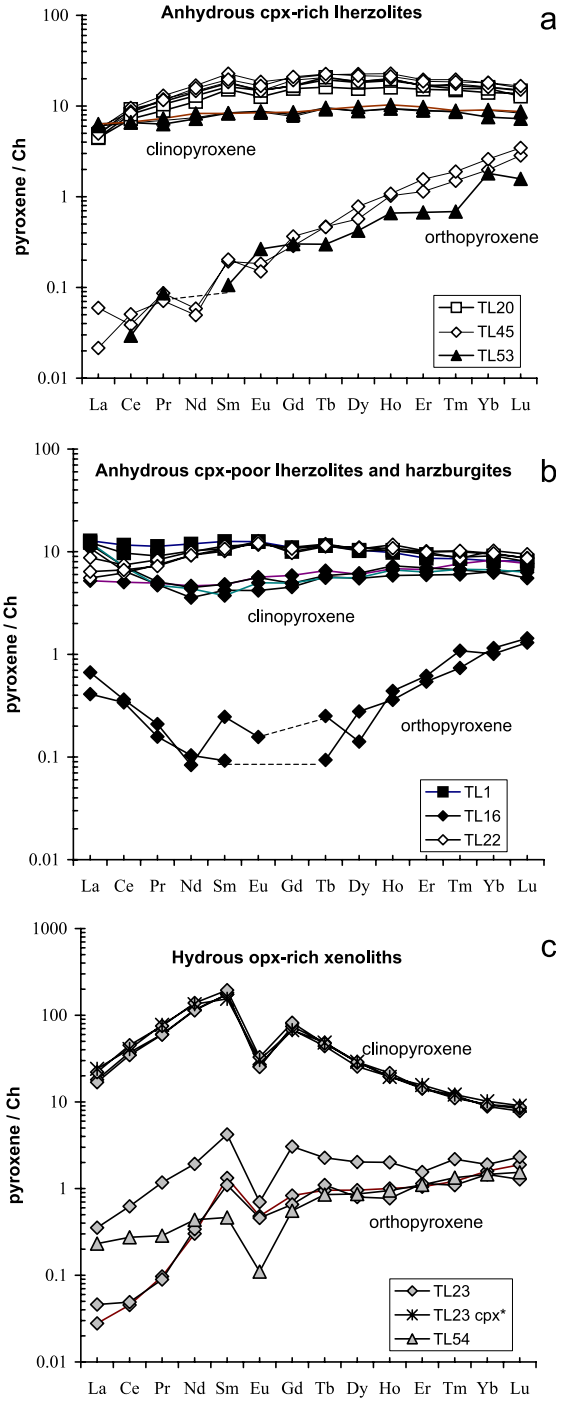

Fig. 5. Chondrite (Ch) normalized REE patterns of individual pyroxene crystals from Tallante mantle xenoliths. TL23 cpx* refers to ICP-MS analysis on a clinopyroxene separate. Normalizing factors from McDonough and Sun (1995).

by hydrous harzburgite and olivine–orthopyroxenite TL 23 and TL 8 ($^{87}Sr/^{86}Sr$ 0.70672–0.70856, and $^{143}Nd/^{144}Nd$ 0.51213–0.51211).

For the anhydrous xenoliths with isotopic composition approaching DM and LREE depletion, Nd model ages (relative to the CHUR) indicate ancient depletion events which most probably occurred in pre-Paleozoic times. On the other hand, anhydrous xenoliths with EMI isotopic signature and LREE enrichment coherently indicate the occurrence of widespread metasomatic processes commonly referred to as "porous flow" percolation of highly alkaline melts (Coltorti et al., 1999, 2000; Beccaluva et al., 2001a,b). These geochemical features are in agreement with the depletion and enrichment events delineated in the comprehensive review of Downes (2001) for the European lithospheric mantle. In particular, a similar isotopic fingerprint is recorded by peridotite xenoliths from Sardinia (Beccaluva et al., 2001a), the Massif Central (Downes and Dupuy, 1987; Zangana et al., 1997) and by some Alpine-type peridotite massifs such as Lherz (Downes et al., 1991), Lanzo (Bodinier et al., 1991), and Ronda (Reisberg et al., 1989 and reference therein).

The peculiar isotopic composition of opx-rich hydrous xenoliths is totally exotic for mantle xenoliths entrained in anorogenic basic magmas, particularly from the circum-Mediterranean region. These data, however, closely approach those of the Neogene calc-alkaline and K-rich volcanics occurring in the Betic Cordillera ($^{87}Sr/^{86}Sr$ 0.70874–0.72073; $^{143}Nd/^{144}Nd$ 0.51242–0.51199; Zeck et al., 1998; Benito et al., 1999; Turner et al., 1999), thus suggesting a possible relationship with subduction-related metasomatic processes. Coherently, in Fig. 7, these opx-rich hydrous xenoliths plot within the subduction-related/hydrous fluid quadrant of Downes (2001), together with the Finero peridotites (Obermiller, 1994).

5. Anorogenic versus subduction-related mantle metasomatism

As reported in the previous sections, different metasomatic effects have been recorded by the Betic subcontinental mantle xenoliths, suggesting the occurrence of at least two types of metasomatizing agents with distinct chemical and isotopic compositions.

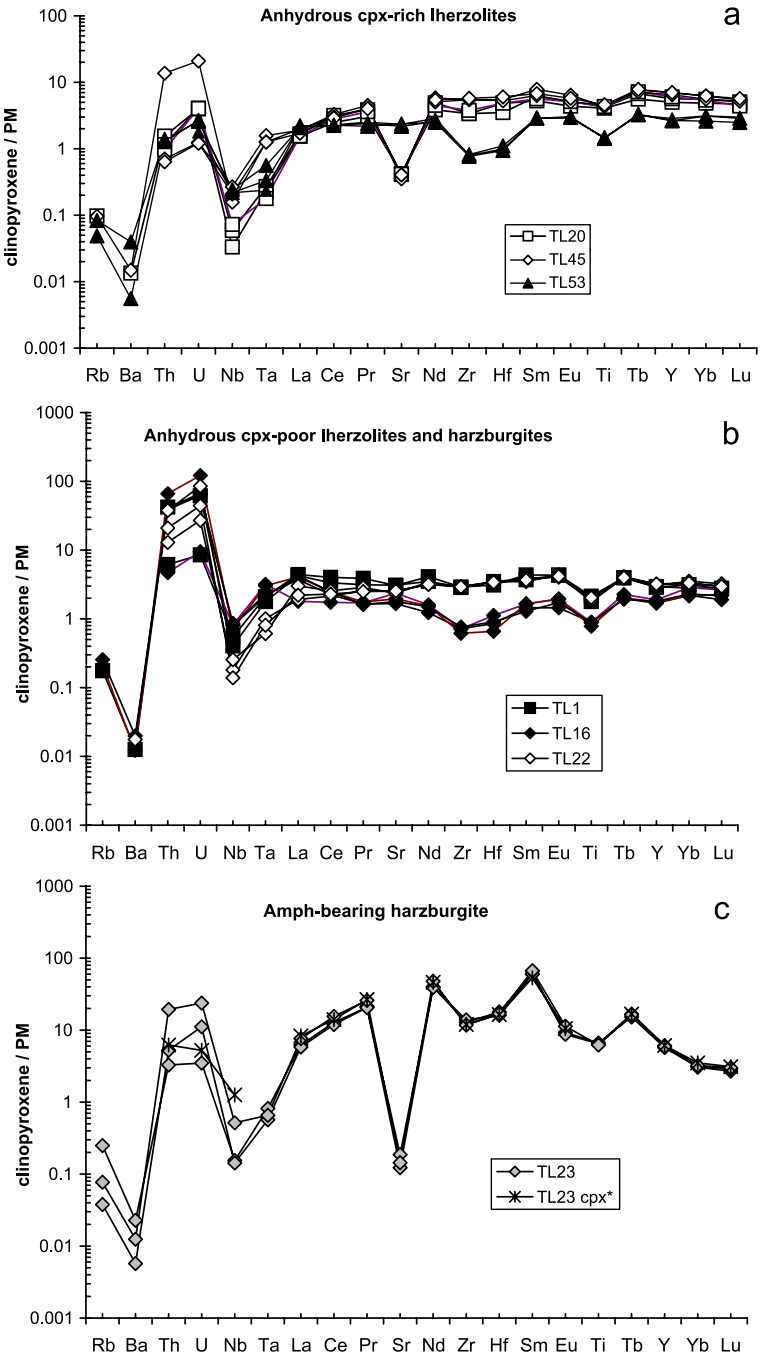

Fig. 6. Primordial mantle (PM) normalized patterns of clinopyroxene individual crystals from Tallante mantle xenoliths. TL23 cpx* refers to ICP-MS analysis on a clinopyroxene separate. Normalizing factors from McDonough and Sun (1995).

Table 4
Sr–Nd isotope compositions of whole-rock (w.r.) and mineral separates (cpx and pl) from Tallante mantle xenoliths and their host lavas

Rock type	Sample	Analysed fraction	$^{87}Sr/^{86}Sr$	$^{143}Nd/^{144}Nd$
Anhydrous peridotite xenoliths				
Hz	TL1	cpx	0.70368	0.51292
Lh	TL14	cpx	0.70213	0.51339
Hz	TL15	cpx	0.70290	0.51283
Lh (cpx poor)	TL16	cpx	0.70413	0.51295
Lh	TL20	cpx	0.70298	0.51310
Lh	TL20	pl	0.70250	
Lh (cpx poor)	TL 22	cpx	0.70302	0.51305
Hz	TL24	cpx	0.70476	0.51250
Lh	TL26	cpx	0.70351	0.51297
Lh	TL45	cpx	0.70272	0.51313
Lh	TL45	pl	0.70265	
Hz	TL52	cpx	0.70296	0.51301
Lh	TL53	cpx	0.70312	0.51306
Hydrous opx-rich xenoliths				
Ol–orth	TL8	w.r.	0.70856	0.51211
Hz	TL 23	cpx	0.70692	0.51213
Hz	TL 23	pl	0.70672	
Host lavas				
Alkaline basalt	TL8 M	w.r.	0.70430	0.51274
Alkaline basalt	TL51 M	w.r.	0.70450	0.51272
Alkaline basalt	B304	w.r.[a]	0.70454	0.51259
Alkaline basalt	1a	w.r.[b]	0.70437	
Alkaline basalt	1b	w.r.[b]	0.70437	

Abbreviations as in Table 1.
[a] Analyses from Turner et al. (1999).
[b] Analyses from Capedri et al. (1989).

The first type of metasomatism appears to have been induced by silica-undersaturated alkaline melts, mainly resulting in variably enriched incompatible elements and Sr–Nd compositions plotting toward EMI. This metasomatism does not show secondary textures, crystallization of new phases, or any significant mineralogical changes in terms of major elements. Therefore, the causative metasomatic processes must have been old enough to attain chemical and textural reequilibration, as also confirmed by the uniform distribution of uranium within individual crystals (Capedri et al., 1989). It is worth noting that chemical and isotopic enrichments have mostly been detected in cpx-poor lherzolites or harzburgites, whereas they are only occasionally recorded in the most fertile lherzolites. This confirms that refractory (cpx-poor) mantle domains are more easily percolated by metasomatizing fluids (Toramaru and Fujii, 1986), and further implies that "porous flow" is the most effective metasomatic mechanism of lithospheric mantle over large within-plate regions. Accordingly, as suggested by Cebrià et al. (2000) and Beccaluva et al. (2001a), anorogenic enrichment events analogous to this metasomatism have widely affected the central–southern portions of the European plate at least since the pre-Middle Mesozoic.

The second metasomatic type is represented by hydrous parageneses with anomalous enrichment in orthopyroxene, suggesting that some lithospheric mantle portions (< 5–10%) beneath the Betic area interacted with silica-oversaturated hydrous melts. This produced local mantle hybridization, with the formation of amphibole/phlogopite-bearing opx-rich (up to 33%) harzburgites containing olivine–orthopyroxenite and gabbronorite lenses. In terms of isotopic composition, this metasomatism is characterized by Sr–Nd values completely different from those recorded in the other xenoliths from Tallante, as they represent the most extreme EM isotopic signature ever found in anorogenic uncontaminated basic magmas and associated mantle xenoliths throughout the European area. These isotopic values, however, approach those of Miocene calc-alkaline and potassic volcanics of the Betic Cordillera, suggesting that they could have been inherited from subduction-derived metasomatizing melts, possibly related to the converging plate system which affected the Betic–Alboran sector during the Tertiary (Benito et al., 1999).

Geochemical modeling was carried out in order to justify the peculiar trace element patterns of both hydrous xenoliths and their constituent pyroxenes, with particular regard to Sr and Eu negative anomalies. These, in fact, cannot be reproduced by pl-peridotite partial melting (Takazawa et al., 2000), nor by alkali-silicate/carbonatite metasomatic enrichments. Calculations (based on incompatible elements of orthopyroxene, clinopyroxene and plagioclase from the well-equilibrated hydrous harzburgite TL23) consistently point to a range of inferred metasomatizing melts which compare most favorably with Betic lamp-

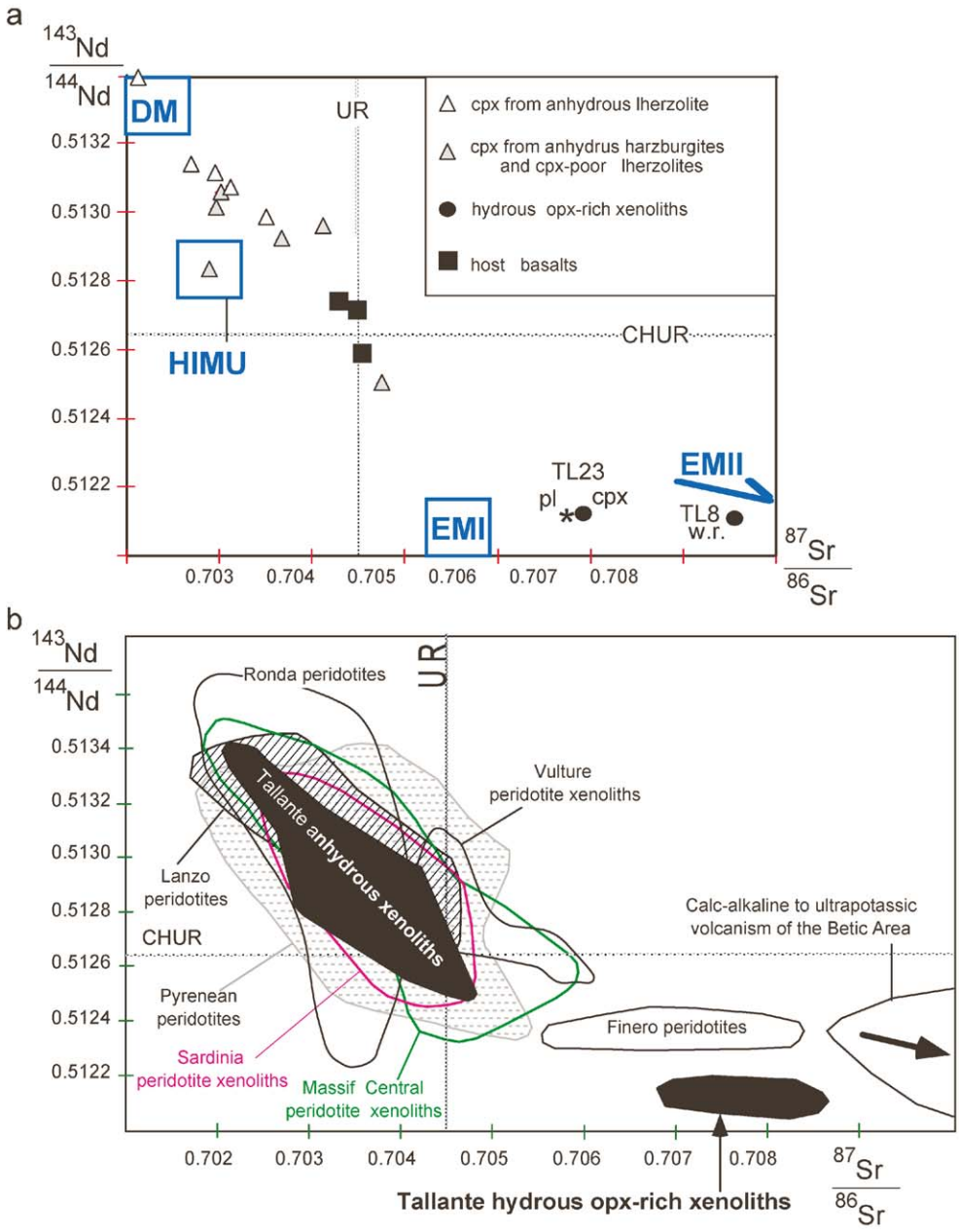

Fig. 7. (a) $^{87}Sr/^{86}Sr$ versus $^{143}Nd/^{144}Nd$ diagram for whole rock (w.r.) and mineral separates (cpx and pl) from Tallante mantle xenoliths, and their host basalts. Mantle end-member components (DM, HIMU, EMI, EMII) are also reported after Zindler and Hart (1986). (b) Compositional fields of other peridotite suites from Central–Western Europe are reported for comparison. Data source for mantle xenoliths: Sardinia, Beccaluva et al. (2001a); Massif Central, Downes and Dupuy (1987) and Zangana et al. (1997); Vulture, Downes et al. (2002). Data source for peridotite massifs: Pyrenees, Downes et al. (1991); Lanzo, Bodinier et al. (1991); Ronda, Reisberg et al. (1989); Finero, Obermiller (1994). Compositional field for calc-alkaline to ultrapotassic lavas of the Betic area is from Turner et al. (1999).

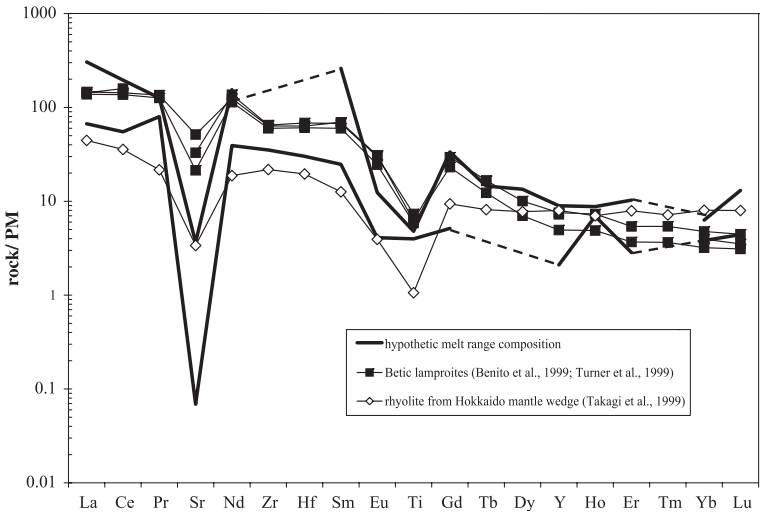

Fig. 8. Primitive mantle (PM) normalized (McDonough and Sun, 1995) incompatible element abundances of the hypothetic melt range in equilibrium with cpx, opx, and pl of the TL23 hydrous harzburgite. Calculations performed using partition coefficients for silica-oversaturated melts: $^{cpx/melt}D$ values from Hill et al. (2000); $^{opx/melt}D$ values for REE from Schwandt and McKay (1998); $^{opx/melt}D$ values for Sr, Zr, Hf, Ti and Y from GERM data set (http://earthref.org/GERM/main.htm); $^{pl/melt}D$ values from Dunn and Sen (1994). Trace element distribution patterns of three Betic lamproites (Turner et al., 1999; Benito et al., 1999) and a rhyolite derived from the Hokkaido mantle wedge (Takagi et al., 1999) are also reported for comparison.

roites, except for a deeper Sr negative anomaly (Fig. 8). Although magmas perfectly corresponding to the computed melts are unknown in the Betic Cordillera, incompatible element patterns (including remarkable Sr negative anomaly) similar to the modeled melts are represented by the Kitami rhyolite from the Hokkaido mantle wedge (Takagi et al., 1999). This suggests that the suprasubduction mantle may have been effectively hybridized by metasomatizing agents that may range in composition from (ultra) potassic silica-oversaturated to rhyodacitic. Besides, the peculiar Sr–Nd isotopic data (coupled with the observed Sr–Eu negative anomalies) suggest that the metasomatizing melts were produced from mantle sources significantly contaminated by subducted terrigenous (continental) components (Beccaluva et al., 1991; Benito et al., 1999; Brandon et al., 1999).

The results from this work, alongside other documented occurrences of subduction-related effects on mantle material, allow us to define some distinctive features of "orogenic" metasomatism as follows:

(1) silica oversaturation of the metasomatizing agent reflected in excess opx crystallization, as also recorded in mantle xenoliths from Papua New Guinea (Grégoire et al., 2001; Franz et al., 2002) and in the subduction-metasomatized Alpine peridotite of Finero (Zanetti et al., 1999); this sometimes results in quartz-bearing felsic veins, as observed in xenoliths from the North Kamchatka arc (Kepezhinskas et al., 1995) and confirmed by experimental constraints (Rapp et al., 1999);
(2) significant departure of the isotopic composition from the anorogenic mantle array, evidenced by high $^{87}Sr/^{86}Sr$ ratios, as also observed in mantle xenoliths from the Philippines (Luzon Arc; Maury et al., 1992), and M. Vulture (South Italy; Downes et al., 2002), as well as at Finero (Hartmann and Wedepohl, 1993; Obermiller, 1994);
(3) particularly high $^{87}Sr/^{86}Sr$ and low $^{143}Nd/^{144}Nd$ ratios, coupled with pronounced Sr–Eu negative anomalies, may indicate a significant contribution of continental terrigenous components in the source of subduction-related metasomatizing agents, as also recorded in mantle xenoliths from Sierra Nevada (Ducea and Saleby, 1998) and Simcoe volcano, WA (Brandon et al., 1999).

An additional, although not exclusive characteristic of subduction-related metasomatism is the significant

presence of phlogopite (and/or amphibole), as also observed in mantle xenoliths from the Philippines (Maury et al., 1992), M. Vulture (Downes et al., 2002), Northern Vulsinian District (Central Italy; Conticelli and Peccerillo, 1990), North Kamchatka (Kepezhinskas et al., 1995), Simcoe volcano (Brandon et al., 1999), Papua New Guinea (Grégoire et al., 2001; Franz et al., 2002) and at Finero.

Acknowledgements

The authors thank for the invaluable assistance provided by Aldo Del Moro during TIMS analyses and Alberto Zanetti during LAM-ICP-MS measurements. Further thanks to Renzo Tassinari for XRF and ICP-MS whole rock analyses, and to Raul Carampin for EPMA analyses. A special thank goes to Massimo Coltorti for the fruitful discussion during the editing of the manuscript. The authors gratefully acknowledge Hilary Downes for her constructive review and Suzanne O'Reilly for the careful editorial comments which led to a significant improvement of the paper.

References

Abe, N., Arai, N., Yurimoto, H., 1998. Geochemical characteristics of the uppermost mantle beneath the Japan Island arc: implication for upper mantle evolution. Phys. Earth Planet. Inter. 107, 233–248.

Banda, E., Gallart, J., Garcia-Duenas, V., Danobeitia, J.J., Makris, J., 1993. Lateral variation of the Crust in the Iberian Peninsula: new evidence from the Betic Cordillera. Tectonophysics 221, 53–66.

Beccaluva, L., Di Girolamo, P., Serri, G., 1991. Petrogenesis and tectonic setting of the Roman Volcanic Province, Italy. Lithos 26, 191–221.

Beccaluva, L., Bianchini, G., Coltorti, M., Del Moro, A., Siena, F., Vaccaro, C., 1999. A case of multistage mantle metasomatism: peridotite xenoliths from Tallante (Southern Spain). Plinius (Eur. J. Mineral. Ital. Suppl.) 22, 41–43.

Beccaluva, L., Bianchini, G., Coltorti, M., Perkins, W.T., Siena, F., Vaccaro, C., Wilson, M., 2001a. Multistage evolution of the European lithospheric mantle: new evidence from Sardinian peridotite xenoliths. Contrib. Mineral. Petrol. 142 (3), 284–297.

Beccaluva, L., Bonadiman, C., Coltorti, M., Salvini, L., Siena, F., 2001b. Depletion events, nature of metasomatizing agent and timing of enrichment processes in lithospheric mantle xenoliths from the Veneto volcanic province. J. Petrol. 42 (1), 173–187.

Beccaluva, L., Bianchini, G., Coltorti, M., Del Moro, A., Siena, F., Vaccaro, C., 2002. A rare case of subduction related metasomatism in mantle xenoliths from the Betic area (South Spain). Geochim. Cosmochim. Acta, Goldschmidt Conf. Spec. Suppl. A59.

Bedini, R.M., Bodinier, J.-L., 1999. Distribution of incompatible trace elements between the constituents of spinel peridotite xenoliths: ICP-MS data from the East African Rift. Geochim. Cosmochim. Acta 63, 3883–3900.

Benito, R., Lòpez Ruiz, J., Cebrià, J.M., Hertogen, J., Doblas, M., Oyarzun, R., Demaiffe, D., 1999. Sr and O isotope constraints on source and crustal contamination in the high-K calc-alkaline and shoshonitic Neogene volcanic rocks of SE Spain. Lithos 46, 773–802.

Bodinier, J.-L., Vasseur, G., Vernières, J., Dupuy, C., Fabriès, J., 1990. Mechanisms of mantle metasomatism: geochemical evidence from the Lherz orogenic massif. J. Petrol. 31, 597–628.

Bodinier, J.-L., Menzies, M.A., Thirlwall, M.F., 1991. Continental to oceanic mantle transition-REE and Sr–Nd isotopic geochemistry of the Lanzo lherzolite massif. J. Petrol., 191–210 (special volume "orogenic lherzolites and mantle processes").

Bottazzi, P., Tiepolo, M., Vannucci, R., Zanetti, A., Brumn, R., Foley, S.F., Oberti, R., 1999. Distinct local configuration for heavy and light REE in amphibole and the prediction of Amph/LiqDREE. Contrib. Mineral. Petrol. 137, 36–45.

Brandon, D.A., Becker, H., Carlson, R.W., Shirey, S.B., 1999. Isotopic constraints on time scales and mechanisms of slab material transport in the mantle wedge: evidence from the Simcoe mantle xenoliths, Washington, USA. Chem. Geol. 160, 387–407.

Brey, G.P., Koehler, T.P., 1990. Geothermobarometry in four phases lherzolites: II. New thermobarometers and practical assessment of existing thermobarometers. J. Petrol. 31, 1353–1378.

Capedri, S., Venturelli, G., Salvioli-Mariani, E., Crawford, A.J., Barbieri, M., 1989. Upper mantle xenoliths and megacrysts in alkali basalts from Tallante, South-Eastern Spain. Eur. J. Mineral. 1, 685–699.

Cebrià, J.M., Lopez-Ruiz, J., Doblas, M., Oyarzun, R., Hertogen, J., Benito, R., 2000. Geochemistry of the Quaternary alkali basalts of Garrotxa (NE volcanic Province, Spain): a case of double enrichment of the mantle lithosphere. J. Volcanol. Geotherm. Res. 102, 217–235.

Coltorti, M., Bonadiman, C., Hinton, R.W., Siena, F., Upton, B.G.J., 1999. Carbonatite metasomatism of the oceanic upper mantle: evidence from clinopyroxene and glasses in ultramafic xenoliths of Grande Comore. Indian Ocean. J. Petrol. 40, 133–165.

Coltorti, M., Beccaluva, L., Bonadiman, C., Salvini, L., Siena, F., 2000. Glasses in mantle xenoliths as geochemical indicator of metasomatic agent. Earth Planet. Sci. Lett. 183 (1–2), 303–320.

Conticelli, S., Peccerillo, A., 1990. Petrological significance of high pressure ultramafic xenoliths from ultra-potassic rocks of Central Italy. Lithos 24, 305–322.

Downes, H., 2001. Formation and modification of the shallow subcontinental lithospheric mantle: a review of geochemical evi-

dence from ultramafic xenolith suites and tectonically emplaced ultramafic massifs of western and central Europe. J. Petrol. 42, 233–250.

Downes, H., Dupuy, C., 1987. Textural, isotopic, and REE variation in spinel peridotite xenoliths, Massif Central, France. Earth Planet. Sci. Lett. 82, 121–135.

Downes, H., Bodinier, J.-L., Thirlwall, M.F., Lorand, J.-P., Fabriès, J., 1991. REE and Sr–Nd isotopic geochemistry of Eastern Pyrenean peridotite massifs: sub-continental lithospheric mantle modified by continental magmatism. J. Petrol., 97–115 (special volume "orogenic lherzolites and mantle processes").

Downes, H., Embey-Isztin, A., Thirwall, M.F., 1992. Petrology and geochemistry of spinel peridotite xenoliths from the western Pannonian Basin (Hungary): evidence for an association between enrichment and texture in the upper mantle. Contrib. Mineral. Petrol. 107, 340–354.

Downes, H., Kostoula, T., Jones, A.P., Beard, A.D., Thirlwall, M.F., Bodinier, J.-L., 2002. Geochemistry and Sr–Nd isotopic composition of mantle xenoliths from the Monte Vulture carbonatite–melilitite volcano, central southern Italy. Contrib. Mineral. Petrol. 144, 78–92.

Ducea, M., Saleby, J., 1998. Crustal recycling beneath continental arcs: silica rich glass inclusions in ultramafic xenoliths from the Sierra Nevada (California). Earth Planet. Sci. Lett. 156, 101–116.

Dunn, T., Sen, C., 1994. Mineral matrix partition coefficients for orthopyroxene, plagioclase and olivine in basaltic to andesitic systems: a combined analytical and experimental study. Geochim. Cosmochim. Acta 58 (2), 717–733.

Dupuy, C., Dostal, J., Boivin, P.A., 1986. Geochemistry of ultramafic xenoliths and their host alkali basalts from Tallante, southern Spain. Mineral. Mag. 50, 231–239.

Franz, L., Becker, K.-P., Kramer, W., Herzig, P., 2002. Metasomatic mantle xenoliths from the Bismark Microplate (Papua New Guinea)—Thermal evolution, geochemistry and extent of slab-induced metasomatism. J. Petrol. 43, 315–343.

Franzini, M., Leoni, L., Saitta, M., 1975. Revisione di una metodologia analitica per fluorescenza X basata sulla correzione degli effetti di matrice. Rend. Soc. Ital. Mineral. Petrol. 31, 365–378.

Green, D.H., Hibberson, W., 1970. The instability of plagioclase in peridotite at high pressure. Lithos 3, 209–221.

Grégoire, M., McInnes, B.I.A., O'Reilley, S.Y., 2001. Hydrous metasomatism of oceanic subarc mantle, Lihir, Papua New Guinea: Part 2. Trace element characteristics of slab-derived fluids. Lithos 59, 91–108.

Hartmann, G., Wedepohl, K.H., 1990. Metasomatically altered peridotite xenoliths from the Hessian Depression (northwest Germany). Geochim. Cosmochim. Acta 54, 71–86.

Hartmann, G., Wedepohl, K.H., 1993. The composition of peridotite tectonites from the Ivrea complex, northern Italy: residues from melt extraction. Geochim. Cosmochim. Acta 57, 1761–1782.

Hill, E., Wood, B.J., Blundy, J.D., 2000. The effect of Ca-Tschermaks component on trace element partitioning between clinopyroxene and silicate melt. Lithos 53, 203–205.

Kepezhinskas, P.K., Defant, M.J., Drummond, M.S., 1995. Na metasomatism in the island arc mantle by slab melt–peridotite interaction: evidence from mantle xenoliths in the North Kamchatka arc. J. Petrol. 36, 1505–1527.

Leoni, L., Saitta, M., 1976. X-ray fluorescence analysis of 29 trace elements in rocks and mineral standards. Rend. Soc. Ital. Mineral. Petrol. 32, 497–510.

Maury, R.C., Defant, M.J., Joron, J.-L., 1992. Metasomatism of the sub-arc mantle inferred from trace elements in Philippine xenoliths. Nature 360, 661–663.

McDonough, W.F., Sun, S., 1995. The composition of the earth. Chem. Geol. 120, 223–253.

Menzies, M.A., Rogers, N., Tindle, A., Hawkesworth, C.J., 1987. Metasomatic and enrichment processes in lithospheric peridotites, an effect of asthenosphere–lithosphere interaction. In: Menzies, M.A, Hawkesworth, C.J. (Eds.), Mantle Metasomatism. Academic Press, London. 472 pp.

Niu, Y., 1997. Mantle melting and melt extraction processes beneath ocean ridges: evidence from abyssal peridotites. J. Petrol. 38, 1047–1074.

Obermiller, W.A., 1994. Chemical and isotopic variations in the Balmuccia, Baldisserro, and Finero peridotite massifs (Ivrea–Zone, N Italy). PhD thesis, Max Planck Institute, Mainz.

O'Reilly, S.Y., Griffin, W.L., 1988. Mantle metasomatism beneath Western Victoria, Australia: I. Metasomatic processes in the Cr-diopside lherzolites. Geochim. Cosmochim. Acta 52, 433–447.

O'Reilly, S.Y., Griffin, W.L., Ryan, C., 1991. Residence of trace elements in metasomatized spinel lherzolite xenoliths: a proton microprobe study. Contrib. Mineral. Petrol. 109, 98–113.

Rapp, R.P., Shimizu, N., Norman, M.D., Applegate, G.S., 1999. Reaction between slab-derived melts and peridotite in the mantle wedge: experimental constraints at 3.8 Gpa. Chem. Geol. 160, 335–356.

Reisberg, L., Zindler, A., Jagoutz, E., 1989. Further Sr and Nd isotopic results from peridotites of the Ronda ultramafic complex. Earth Planet. Sci. Lett. 96, 161–180.

Schwandt, C.S., McKay, G.A., 1998. Rare earth element partition coefficients from enstatite-melt synthesis experiments. Geochim. Cosmochim. Acta 62, 2845–2848.

Siena, F., Beccaluva, L., Coltorti, M., Marchesi, S., Morra, V., 1991. Ridge to hot-spot evolution of the Atlantic lithospheric mantle: evidence from Lanzarote peridotite xenoliths (Canary Islands). J. Petrol., 271–290 (special volume "orogenic lherzolites and mantle processes").

Takagi, T., Oriahashi, Y., Naito, K., Watanabe, Y., 1999. Petrology of a mantle-derived rhyolite, Hokkaido, Japan. Chem. Geol. 160, 425–445.

Takahashi, E., 1986. Genesis of calc-alkaline andesite magma in a hydrous mantle–crust boundary: petrology of lherzolite xenoliths from the Ichinomegata Crater, Oga Peninsula, Northeast Japan, Part II. J. Volcanol. Geotherm. Res. 29, 355–395.

Takazawa, E., Frey, F.A., Shimizu, N., Obata, M., 2000. Whole rock compositional variations in an upper mantle peridotite (Horoman, Hokkaido, Japan): are they consistent with a partial mantle process? Geochim. Cosmochim. Acta 64, 695–716.

Tiepolo, M., Bottazzi, P., Palenzona, M., 2003. A laser probe coupled with ICP-double-focusing sector -field mass spectrometer for in situ analysis of geological samples and U–Pb dating of zircon. Can. Miner 41, 259–272.

Toramaru, A., Fujii, N., 1986. Connectivity of melt phase in a partially molten Peridotite. J. Geophys. Res. 91, 9239–9252.

Turner, S.P., Platt, J.P., George, R.M.M., Kelley, S.P., Pearson, D.G., Nowell, G.M., 1999. Magmatism associated with orogenic collapse of the Betic–Alboran domain, SE Spain. J. Petrol. 40, 1011–1036.

Vaselli, O., Downes, H., Thirlwall, M.F., Dobosi, G., Coradossi, N., Seghedi, I., Szakacs, A., Vannucci, R., 1995. Ultramafic xenoliths from Plio–Pleistocene alkali basalts from the Eastern Transylvanian Basin: depleted mantle enriched by vein metasomatism. J. Petrol. 38, 23–54.

Vaselli, O., Downes, H., Thirlwall, M.F., Vannucci, R., Coradossi, N., 1996. Spinel–peridotite xenoliths from Kapfenstein (Graz Basin, Eastern Austria): a geochemical and petrological study. Mineral. Petrol. 57, 23–50.

Zanetti, A., Mazzuchelli, M., Rivalenti, G., Vannucci, R., 1999. The Finero phlogopite massif: an example of subduction-related metasomatism. Contrib. Mineral. Petrol. 134, 107–122.

Zangana, N.A., Downes, H., Thirlwall, M.F., Hegner, E., 1997. Relationship between deformation, equilibration temperatures, REE and radiogenic isotopes in mantle xenoliths (Ray Pic, Massif Central, France): an example of plume–lithosphere interaction? Contrib. Mineral. Petrol. 127, 187–203.

Zangana, N.A., Downes, H., Thirlwall, M.F., Marriner, G.F., Bea, F., 1998. Geochemical variation in peridotite xenoliths and their constituent clinopyroxenes from Ray Pic (French Massif Central): implications for the composition of the shallow lithospheric mantle. Chem. Geol. 153, 11–35.

Zeck, H.P., Kristensen, A.B., Williams, I.S., 1998. Post collisional volcanism in a sinking slab setting-crustal anatectic origin of pyroxene–andesite magma, Caldear Volcanic Group, Neogene Alboran volcanic province, southeastern Spain. Lithos 45, 499–522.

Zindler, A., Hart, S.R., 1986. Chemical geodynamics. Ann. Rev. Earth Planet. Sci. Lett. 14, 493–571.